nature communications

Article

https://doi.org/10.1038/s41467-025-58367-4

Engineered circular guide RNAs enhance miniature CRISPR/Cas12f-based gene activation and adenine base editing

Received: 15 May 2024

Accepted: 18 March 2025

Published online: 28 March 2025

Check for updates

Xin Zhang[1,2,5], Mengrao Li[1,5], Kechen Chen[1], Yuchen Liu[1], Jiawei Liu[1], Jiahong Wang[1], Hongxin Huang[1], Yanqun Zhang[1], Tao Huang[3], Shufeng Ma[1,2], Kaitong Liao[1], Jiayi Zhou[1], Mei Wang[4], Ying Lin[1] ✉ & Zhili Rong[1] ✉

CRISPR system has been widely used due to its precision and versatility in gene editing. Un1Cas12f1 from uncultured archaeon (hereafter referred to as Cas12f), known for its compact size (529 aa), exhibits obvious delivery advantage for gene editing in vitro and in vivo. However, its activity remains suboptimal. In this study, we engineer circular guide RNA (cgRNA) for Cas12f and significantly improve the efficiency of gene activation about 1.9–19.2-fold. When combined with a phase separation system, the activation efficiency is further increased about 2.3–3.9-fold. In addition, cgRNA enhances the editing efficiency and narrows the editing window of adenine base editing about 1.2–2.5-fold. Importantly, this optimization strategy also boosts the Cas12f-induced gene activation efficiency in mouse liver. Therefore, we demonstrate that cgRNA is able to enhance Cas12f-based gene activation and adenine base editing, which holds great potential for gene therapy.

The clustered regularly interspaced short palindromic repeats (CRISPR) and CRISPR-associated proteins (Cas), integral to the adaptive immune system in bacteria and archaea, serve as a defense mechanism against phage infections[1–3]. This system has been harnessed for diverse applications, including DNA or RNA cleavage[4,5], regulation of gene expression[6,7], base editing[8,9], and live-cell imaging[10,11], among others[12–14]. Its versatility extends to various fields, such as constructing animal and plant models, advancing drug development, and contributing significantly to disease research and therapeutics[15,16]. The CRISPR/Cas12f system, especially noted for its remarkably compact size, stands as a fascinating facet of CRISPR technology. The system encompasses variants like Un1Cas12f1 from uncultured archaeon[17,18], *Acidibacillus sulfuroxidans* Cas12f1 (*As*Cas12f1)[19], *Oscillibacter sp.* Cas12f1 (*Os*Cas12f)[20], and *Ruminiclostridium herbifermentans* Cas12f1 (*Rh*Cas12f1)[20], with only 400–600 amino acids and much smaller than other Cas proteins like Cas9 and Cas12a[21]. The compact nature of Cas12f enhances its delivery efficiency, making it highly promising for both in vivo and in vitro applications[22,23], similar to other miniature nucleases[9,24–26]. However, Cas12f displays much lower gene-editing activity than the widely used Cas9 and Cas12a.

To improve the gene-editing efficiency of the CRISPR/Cas12f system, the Cas12f protein and gRNA have been engineered. Directed by the structure of the Cas12f/gRNA/DNA complex, Cas12f nuclease has been mutated at specific site or by deep mutational scanning, and gRNA has been reformed by fine-tuning the length and scaffold sequence, which has optimized the interaction between Cas12f and gRNA and enhanced gene-editing activity[17–19,27]. In spite of these

[1]Cancer Research Institute, School of Basic Medical Sciences, State Key Laboratory of Multi-organ Injury Prevention and Treatment, Guangdong Province Key Laboratory of Immune Regulation and Immunotherapy, Southern Medical University, Guangzhou, China. [2]State Key Laboratory of Respiratory Disease, National Clinical Research Center for Respiratory Disease, National Center for Respiratory Medicine, Guangzhou Institute of Respiratory Health, the First Affiliated Hospital of Guangzhou Medical University, Guangzhou, China. [3]Dermatology Hospital, Southern Medical University, Guangzhou, China. [4]Department of Developmental Biology, School of Basic Medical Sciences, Southern Medical University, Guangzhou, China. [5]These authors contributed equally: Xin Zhang, Mengrao Li. ✉e-mail: linying0216@smu.edu.cn; rongzhili@smu.edu.cn

advancements, the gene-editing efficiency of Cas12f has not yet reached the level of more widely used Cas9 and Cas12a[28].

Guide RNA is a critical component of the CRISPR system, essential for directing the Cas proteins to the specific DNA or RNA sequence. Traditional gRNAs, being linear, exhibit a significantly shorter half-life compared to Cas proteins, which severely limit the efficiency in the gene editing process[29]. However, circular RNAs, characterized by their covalently closed loop structure, offer enhanced protection against exonuclease degradation, resulting in greater stability[30–33]. Recent studies have demonstrated that engineered circular ADAR-recruiting RNAs can substantially increase RNA editing efficiency and fidelity[34,35]. In the context of CRISPR/Cas9, circular guide RNAs have been shown to improve editing efficiency in vitro and in bacteria[36]. Similarly, within CRISPR/Cas12a and CRISPR/Cas13d systems, circular gRNAs have exhibited increased stability, which promotes the accumulation of unbound gRNA, and facilitates its self-processing by Cas12a or Cas13d into mature protein/gRNA complexes, thereby markedly enhancing the efficiency of both DNA and RNA editing processes[37,38].

In this study, we design and optimize a circular gRNA specifically tailored for *Un1*Cas12f-ge4.0 (hereafter referred to as Cas12f), which significantly enhances both the gene activation efficiency and adenine base editing efficiency.

Results

Circular guide RNAs (cgRNAs) with increased stability activate reporter genes in the CRISPR/Cas12f system

In order to improve the stability of gRNA, we tried to construct cgRNA using the Tornado expression system similar as previous description[30] (Fig. 1a). Real-time reverse transcription PCR (RT-PCR) assay with two outward-facing primers confirmed the circularization of cgRNA (Circular), which was not observed for normal gRNA (Normal) or linear gRNA (Linear) (Fig. 1b). RT-PCR quantification revealed that the expression level of circular gRNA was about 392.9-fold and 194.6-fold higher than that of normal and linear gRNA, respectively (Fig. 1c). Additionally, using actinomycin D treatment to inhibit RNA transcription, we further ascertained that cgRNA was more stable than Normal gRNA (Fig. 1d). Next, to directly assess the effect of cgRNA on gene editing, we constructed two reporter cell lines, which expressed doxycycline-inducible dCas12f-VPR fusion protein and Cas/gRNA-activatable mNeonGreen protein (namely G3 or G5 reporter cell lines). Upon the addition of doxycycline (DOX) and transfection with proper gRNA plasmids, the downstream mNeonGreen gene expression was activated (Supplementary Fig. 1a–c). Fluorescence-activated cell sorting (FACS) assay showed that cgRNA, with a 19-nt spacer and 10-nt linker1 and linker2, significantly enhanced activation efficiency compared with Normal and Linear gRNAs in both G3 and G5 reporter cell lines (Fig. 1e, f, Supplementary Fig. 1d). All the above data demonstrated that cgRNA increased the stability of gRNA and thus the gene-activation efficiency in human cells.

Optimization of the Cas12f/cgRNA system

Next, we tried to optimize the Cas12f/cgRNA system. Dose-dependent analyses showed that cgRNA significantly activated the expression of mNeonGreen in the G3 and G5 reporter cells from 8 to 500 ng in 24-well plates and cgRNA displayed a superior capability for gene activation when compared to Normal gRNA (Fig. 2a; Supplementary Figs. 2, 3). Time-course analyses showed that cgRNA significantly activated gene expression from Days 1 to 7 while Normal gRNA almost failed to activate gene after Day 6 and thus cgRNA exhibited better durability than Normal gRNA (Fig. 2b; Supplementary Figs. 4, 5).

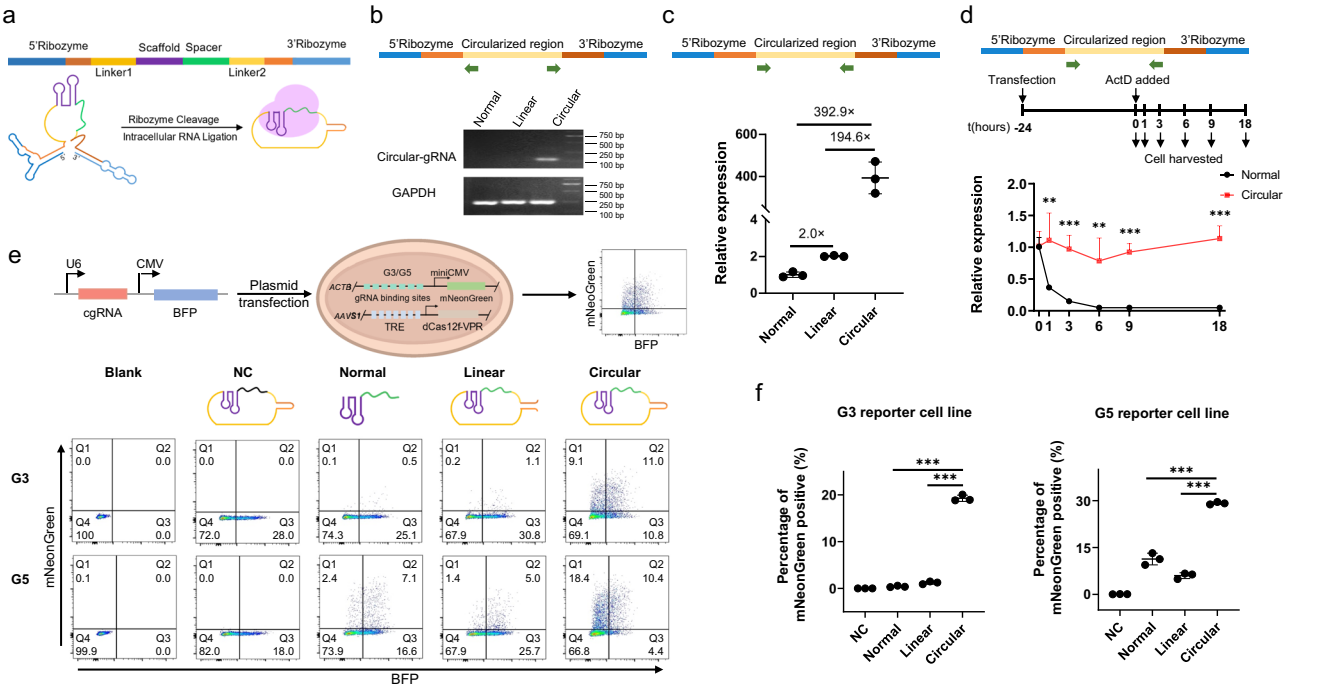

Fig. 1 | Circular guide RNAs (cgRNAs) with increased stability activate reporter genes in the CRISPR/Cas12f system. a Schematic representation of circular gRNA for CRISPR/Cas12f. **b** Reverse transcription PCR (RT-PCR) confirmation of RNA circularization in cells. **c** RT-PCR analysis revealed the abundance of circular RNAs in cells. HEK293T cells were transfected with indicated plasmids encoding normal, linear or circular RNAs, and 48 h post-transfection, RNA was harvested for RT-PCR analysis. **d** RT-PCR analysis of RNA stability. Cells transfected with gRNAs were treated with actinomycin D for 1, 3, 6, 9, and 18 h, starting 24 h post-transfection. **e** Fluorescence-activated Cell Sorting (FACS) analysis revealing mNeonGreen expression in reporter cells three days post-transfection with G3 or G5 gRNA plasmids. **f** Quantification of activation efficiency by the ratio of mNeonGreen-positive cells in FACS assays. For **c**–**f** $n = 3$ independent experiments, and data are presented as mean values ± SD. Normal, normal gRNAs driven by the polymerase III promoter U6; Circular, circular gRNA driven by the polymerase III promoter U6; Linear, linear gRNA having the same base residues as the circular gRNA; NC, non-targeting gRNA which transfected gRNA plasmids do not target any site in the human genome or transcriptome. $^{**}p < 0.01$, $^{***}p < 0.001$, two-sided Student's *t*-test. Source data are provided as a Source Data file.

https://doi.org/10.1038/s41467-025-58367-4

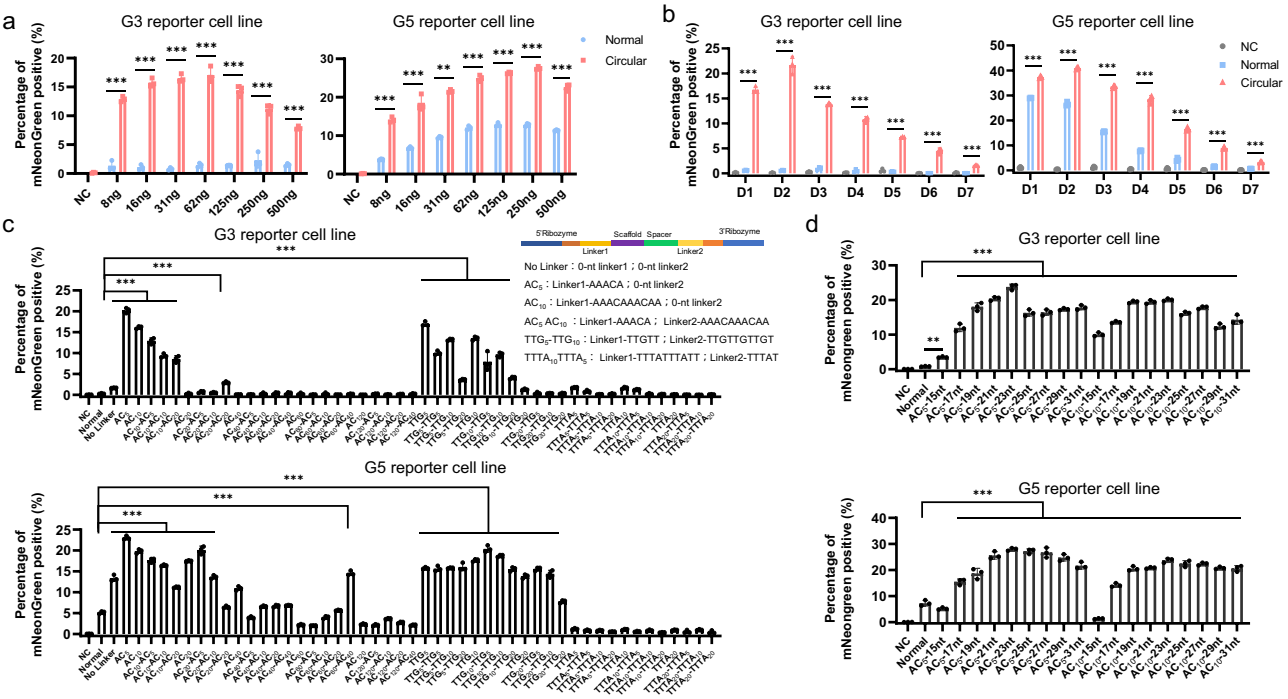

Fig. 2 | Optimization of the Cas12f/cgRNA system. a Dose-dependent analysis of cgRNA-directed gene activation in the reporter cells two days after transfection. **b** Time-course analysis of cgRNA-directed gene activation in the reporter cells transfected with 16 ng cgRNAs. **c** Gene activation guided by cgRNAs with various linkers in the reporter cells three days after transfection with 16 ng cgRNAs. **d** Gene activation guided by cgRNAs with various lengths combined with the linker AC_5 and AC_{10} in the reporter cells three days after transfection with 16 ng cgRNAs. AC_5-15nt refers to the length of spacer sequence is 15nt and the AC_5 linker is used. For **a**–**d** $n = 3$ independent experiments, and data are presented as mean values ± SD. $^*p < 0.05$, $^{**}p < 0.01$, $^{***}p < 0.001$, (two-sided Student's *t*-test for (**a**) and (**b**) one-way ANOVA *t*est for **c** and **d** tested sample versus Normal gRNA sample). Source data are provided as a Source Data file.

Because the structure of cgRNA was essential to their target recognition and function, we tested different flexible RNA linker1 between 5′ ribozyme and gRNA scaffold and linker2 between gRNA spacer and 3′ ribozyme. The adenine- and cytosine-rich (poly-AC) sequence, frequently utilized as a flexible RNA linker, has been shown to enhance RNA function[35,37]. Additionally, previous study has shown that a poly (uridinylated) (U-rich) 3′ overhang on the crRNA increased Cas12f-mediated editing efficiency[17]. Therefore, we incorporated flexible poly-AC and poly- U RNA linkers to flanking cgRNA. FACS assays showed that 5-nucleotide or 10-nucleotide flexible poly-AC RNA linkers between 5′ ribozyme and gRNA scaffold, termed AC_5 and AC_{10}, performed as two of the best among all the tested linkers (Fig. 2c; Supplementary Figs. 6, 7). Finally, we tested the length of spacer sequence and found that 23-nt was optimal (Fig. 2d; Supplementary Figs. 8, 9). In summary, cgRNA with AC_5 linker and 23-nt spacer sequence showed higher activation efficiency than Normal gRNA in the reporter cells, particularly under conditions of low concentration and prolonged duration.

Activation of endogenous genes using the Cas12f/cgRNA system

Next, we explored whether cgRNAs could enhance dCas12f-based endogenous gene activation. In a doxycycline-inducible dCas12f-VPR knock-in (KI) HEK293T cell line (Supplementary Fig. 10), plasmids encoding gRNAs were transiently transfected to activate *IL1RN, HBG, HBB, ASCL1, RHXOF2, and CD2* gene expression. RT-PCR analysis showed that cgRNAs were more potent than Normal and linear gRNAs, with about 1.9–19.2-fold and 2.9–56.6-fold, respectively (Fig. 3a). We also co-transfected plasmids encoding dCas12f-VPR and gRNAs into the breast cancer cell line MCF7 and the myeloid cell lines THP1 and MV4-11, similar results were observed (Fig. 3b). Finally, the specificity of cgRNAs-mediated gene activation was examined by RNA-seq analyses. As shown in Fig. 3c, cgRNAs exhibited about 18.1-fold and 27.4-fold increases compared to Normal gRNA and Linear gRNA, respectively. And 23, 15, and ten genes other than the target *HBG* gene were observed up-regulated in the cgRNA group when compared to the NC, Normal, and Linear groups (Deseq2, $q < 0.05$), indicating a slight lower specificity (Fig. 3c). In summary, cgRNAs could significantly enhance endogenous gene activation with high efficiency and specificity in human cells.

Furthermore, we assessed the effect of the Cas12f/cgRNA-4.1 system. Consistent with the Cas12f/gRNA-4.0 results, circular gRNAs significantly enhanced the activation efficiency of the mNeonGreen gene in reporter cell lines, as well as the endogenous *HBG* and *HBB* genes in HEK293T cells (Supplementary Fig. 11).

Phase separation enhances the Cas12f/cgRNA system-induced gene activation

Transcription factors and coactivators could form dynamic compartmentalization organelles via liquid–liquid phase separation to regulate transcription[39]. Our and other group's previous work has revealed that phase-separation could improve the efficiency of CRISPR-mediated transcriptional activation[40,41]. Therefore, we tried to fuse a phase-separation domain FUS^{IDR} (the intrinsically disordered region (IDR) of FUS protein) with dCas12f-VPR to further increase the efficiency of Cas12f/ cgRNA gene activation system (Fig. 4a). RT-PCR analyses displayed that the expression of the target gene *HBG1* and *HBB* could be further activated to about 2.2–3.9-fold when FUS^{IDR} domain was fused to the C-terminal of dCas12f-VPR (Fig. 4b). To test whether dCas12f-VPR-FUS^{IDR} could undergo phase separation, we transfected plasmid encoding dCas12f-VPR-FUS^{IDR}-sfGFP or dCas12f-VPR-sfGFP into HEK293T cells and found that dCas12f-VPR-sfGFP distributed evenly in the nucleus while dCas12f-VPR-FUS^{IDR}-sfGFP formed droplets (Fig. 4c). Further, fluorescence recovery after photobleaching (FRAP) experiments demonstrated that these dCas12f-VPR-FUS^{IDR}-sfGFP droplets exhibited high mobility, a major feature of liquid-liquid phase separation (Fig. 4d).

https://doi.org/10.1038/s41467-025-58367-4

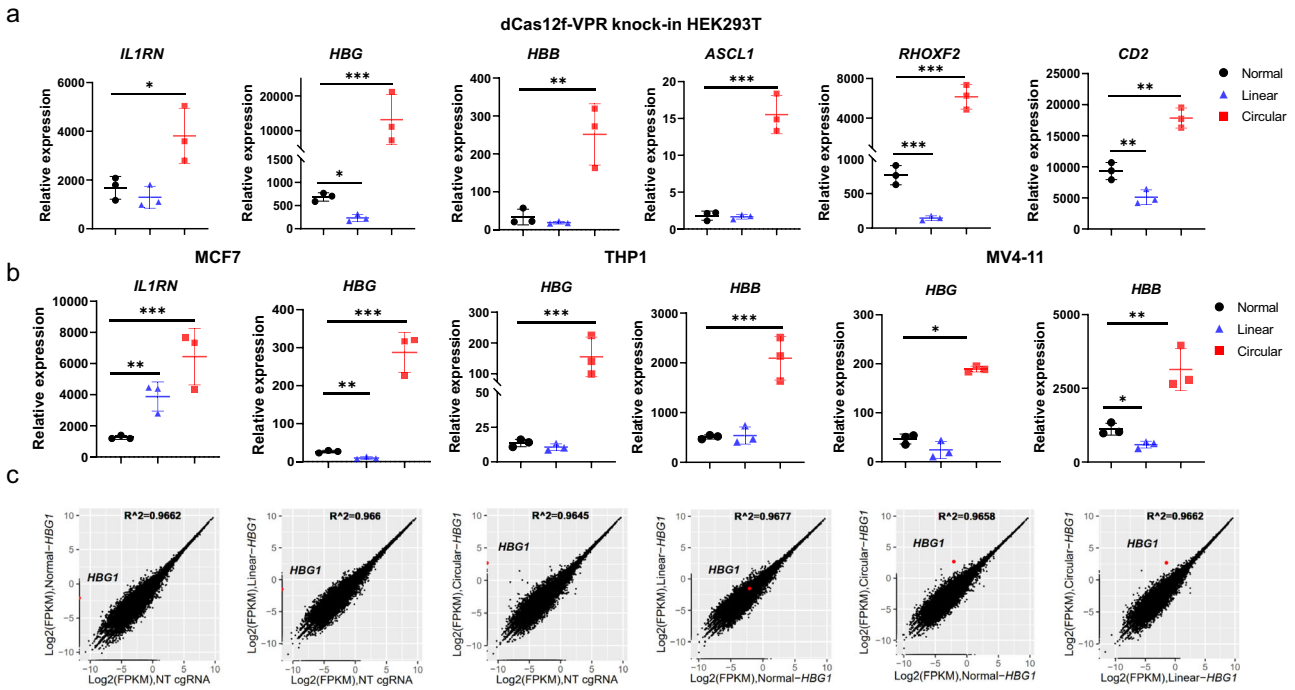

Fig. 3 | Activation of endogenous genes using the Cas12f/cgRNA system. **a** Targeted gene activation guided by Normal, linear, and circular gRNAs in the dCas12f-VPR knock-in (KI) HEK293T cell line transfected with 16 ng gRNAs. Data are presented as mean values ± SD. **b** Targeted gene activation guided by Normal, linear and circular gRNAs in MCF7, THP1, and MV4-11 cell lines transiently co-transfected with dCas12f-VPR and gRNA-encoded plasmids. Data are presented as mean values ± SD. **c** Specificity of gene activation by the Cas12f/cgRNA system. Gene expression profiles derived from RNA-seq data of KI HEK293T cells transfected with normal, linear, and circular gRNAs targeting *HBG1*, and cgRNAs targeting mNeonGreen (negative control, NC). For **a**–**c**, $n = 3$ independent experiments, $^{*}p < 0.05$, $^{**}p < 0.01$, $^{***}p < 0.001$, one-way ANOVA test. Source data are provided as a Source Data file.

Circular gRNAs improve the efficiency and narrow the editing window of adenine base editing

Next, we checked whether cgRNA could boost Cas12f-induced genomic DNA cleavage. As shown in Supplementary Fig. 12, U6-derived normal gRNA induced obvious indels at *SITE1* and *CLIC4* sites revealed by Sanger-seq, however, to our surprise, cgRNA induced no indels at the same site. Thus, we found that cgRNA/Cas12f complex could enhance gene activation but lose DNA cleavage activity (Supplementary Fig. 12). It has been reported that conformation change after gRNA/Cas12f complex binding to the target site is essential for DNA cleavage[42], therefore we speculated that cgRNA/Cas12f complex retained the DNA binding capability to activate gene activation but might lose the ability for conformation change and thus failed to cleavage target DNA.

Recent studies have revealed that Cas12f-mediated base editors were well suited for AAV packaging and hold great potential to correct disease-causing mutations[18]. It has been reported that both Cas nickase mutants (nCas proteins) and nuclease-dead mutants (dCas proteins) could be used for base editing, but nCas proteins generally exhibit higher efficiency. Therefore, we next tested whether cgRNAs could enhance the performance of dCas12f-mediated base editing. Although the cgRNA/Cas12f complex failed to induce indels, it was very low possibility that this complex performed as a nickase, and therefore we also used wide type Cas12f for base editing test. Therefore, we tested whether Cas12f could be used for adenine base editing (ABE). As shown in Fig. 5a, we fused a heterodimer TadA-TadA* on the C-terminal of dCas12f and Cas12f. Sanger-seq analysis showed that cgRNAs with AC_5 or AC_{10} linker could induce A-T to G-C conversion at A3 location on the *GS1* and *VEGFA* target sites in both dCas12f-ABE and WT Cas12f-ABE systems (the R in the TTTR PAM was defined as site 0, Supplementary Fig. 13). To determine the editing efficiency at each position, Deep-seq was employed to check base frequency at each site cross about 150 bp around the target site, and the results showed that the total A-T to G-C conversion efficiency of cgRNAs exhibited up to about 26.6%, about 1.2–2.5-fold increase compared with Normal gRNAs, at the tested nine sites (Fig. 5b). It was noticed that dCas12f-ABE performed better than Cas12f-ABE, and that cgRNAs with AC_5 or AC_{10} linkers exhibited variable performance across different target sites (Fig. 5b).

We further analyzed the editing window. As shown in Fig. 5c, A3 and A4 locations were the major editing locations at each target site with either dCas12f-ABE or Cas12f-ABE with either gRNA type. More importantly, we found that cgRNA with either AC_5 or AC_{10} linker showed much narrow editing window with about 56.61% to 97.0% (average 81.9%) at A3/A4 location while normal gRNA only induced about 29.1% to 79.5% (average 54.0%) at A3/A4 location, in the tested nine sites (Fig. 5c, d, Supplementary Fig. 14). cgRNA-induced narrow editing window suggested much less bystander editing events and thus a much more precise editing, which could increase the safety guaranty of therapeutic ABE. Finally, we checked the editing purity. No base change other than A-T to G-C was observed (Supplementary Fig. 15a), but obvious indels were observed only in the normal gRNA-guided, and much less but detectable in the linear gRNA-guided, WT Cas12f-ABE system at the *FUS*, *LOC105370393*, *INIP*, *GS1*, and *VEGFA* sites, which was also consistent with that cgRNA/Cas12f failed to cleavage DNA (Fig. 5e and Supplementary Fig. 15b).

In summary, cgRNA-guided dCas12f-ABE showed high efficiency and precision (narrow editing window, undetectable other base change and indels), which could facilitate the installation of therapeutic adenine base editing.

Circular gRNAs enhance Cas12f-based transcriptional activation in vivo

We also explored whether cgRNAs could improve gene activation in vivo. Firstly, the plasmids TRE-Luciferase-ployA and dCas12f-VPR, and different doses of gRNA plasmids targeting the TRE promoter were transiently co-transfected into human HEK293T cells (Fig. 6a).

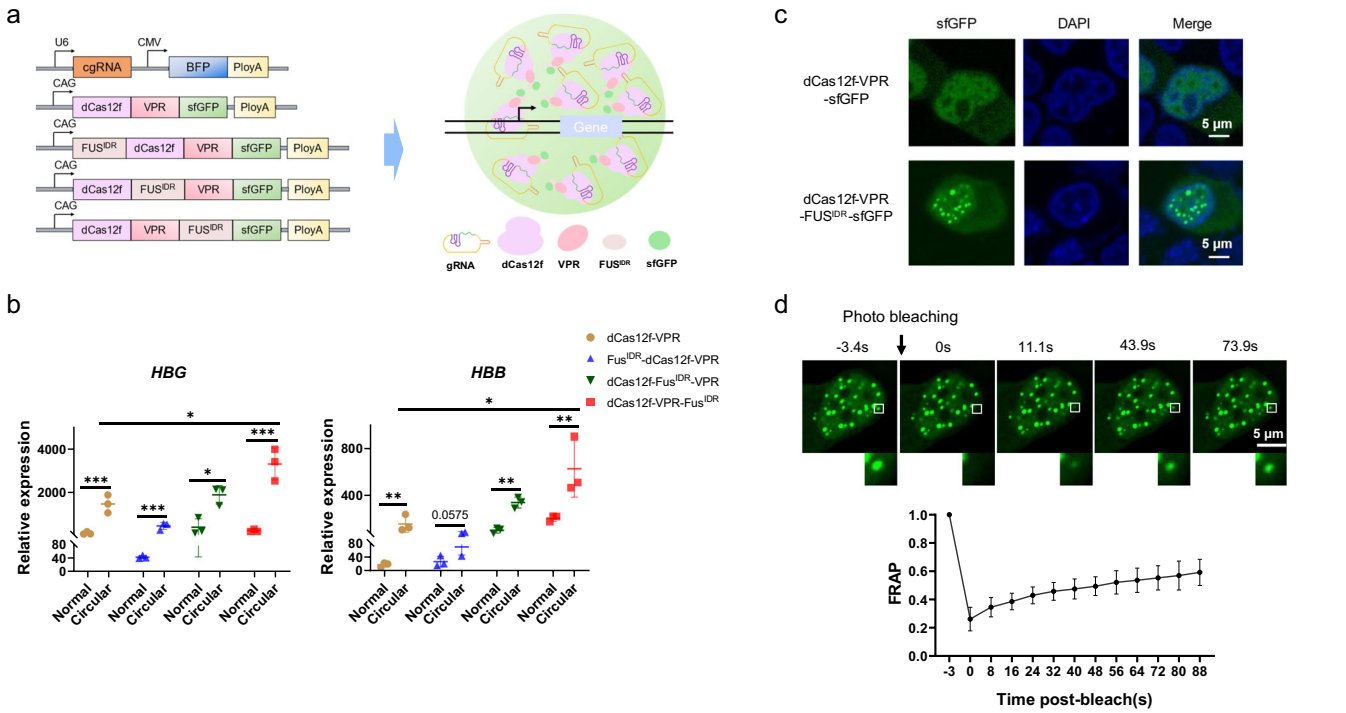

Fig. 4 | Phase separation enhances the Cas12f/cgRNA system-induced gene activation. a Schematic diagram of the phase-separated activation using the Cas12f/cgRNA system. **b** RT-PCR analysis showed relative mRNA expression of targeted gene in HEK293T cells utilizing the Cas12f/cgRNA system combined with phase separation system. Data are plotted as mean ± SD ($n = 3$ independent experiments), $^{*}p < 0.05$, $^{**}p < 0.01$, $^{***}p < 0.001$, two-sided Student's *t*-test. **c** GFP fluorescence in HEK293T cells transfected with dCas12f-VPR-sfGFP or dCas12f-VPR-FUS^{IDR}-sfGFP plasmid. $n = 5$ independent experiments, Scale bar, 5 μm. **d** The fluorescence recovery after photobleaching (FRAP) analysis of dCas12f-VPR-FUS-sfGFP droplets in HEK293T cells. Scale bar, 5 μm. Data are plotted as mean ± SD ($n = 5$ independent experiments). Source data are provided as a Source Data file.

After 3 days, D-Luciferin was added into the media to examine the activity of luciferase. Bioluminescence image and quantification analysis showed the cgRNAs could induce luciferase activation better than Normal gRNAs in the cell cultures (Fig. 6b, c). Next, we co-delivered the three plasmids to the mouse liver via hydrodynamic tail vein injection (HTVI) and monitored luciferase activity for nine days (Fig. 6d). Similarly, cgRNAs outperformed Normal gRNAs at each time point with about 3.3–19.3-fold change (Fig. 6e, f).

Discussion

In this study, we employed the Tornado expression system to generate cgRNAs that were more stable and performed better than their linear counterparts in the miniature Un1Cas12f-ge4.0 system. The cgRNAs significantly improved the gene activation efficiency and the integration of phase separation further enhanced this effect. Moreover, cgRNAs could increase the efficiency and narrow the editing window of A-to-G base editing. Finally, cgRNA also boosted Cas12f-based gene activation in adult mouse liver.

The miniature gene editing system, including Cas12f, TnpB, and IscB families, can be delivered more easier than the widely used Cas9 and Cas12a, making it great promising for therapeutic gene editing in vivo. However, the low editing efficiency severely restricts their applications. In this study, we demonstrated that circularization of gRNA could significantly increase the efficiency of gene activation of Cas12f, achieving relative long durable editing period even with minimal amount of cgRNAs, which were two critical points for therapeutic gene editing in vivo. Our group has previously reported that cgRNA is able to enhance the efficiency of gene activation and DNA cleavage of Cas12a as well as phase separation can boost CRISPR-based gene activation systems[37]. In this study, we found that combination of cgRNA and phase separation could further increase the efficiency of gene activation, indicating that cgRNA could be compatible with other strategies to further optimize the miniature system. Therefore, we believe that integrating cgRNA with other optimization strategies, like Cas protein mutants with high activity and another more powerful effector for gene activation or base editing, might further improve the performance of the Cas12f/cgRNA system.

More interestingly, the Cas12f/cgRNA-ABE system displayed not only increased activity but also narrowed editing window (Fig. 5). In addition, no base change other than A-to-G was detected and no indels was detected in the cgRNA guided ABE system (Fig. 5). These findings guaranteed that the Cas12f/cgRNA-ABE system was an ideal tool for high efficiency and precise adenine base editing for therapeutic purposes. As well-known, in principle, about 50% of genetic diseases could be treated by ABE, much more than that could be treated by Cytosine base editors (CBE)[43]. Thus, in addition to the compact size to facilitate delivery, the Cas12f/cgRNA-ABE system holds great promise for therapeutic applications.

Although, we failed to discover a proper condition to enhance DNA cleavage by cgRNAs, we did find conditions to enhance gene activation and ABE, which were nuclease activity independent but target site recognition and binding dependent. Therefore, in theory, the installation of other functions that do not require nuclease activity, such as gene repression, epigenetic modulation, live-cell imaging, and chromatin loop reorganization, might be achieved by cgRNA.

Unlike Cas12a and Cas13d, Cas12f probably lacks the ability for self-processing of gRNA, rendering it unable to convert circular gRNA into its mature gRNA[44]. And the secondary structure of cgRNA plays a crucial role in both forming the correct protein/gRNA complex and facilitating target gene recognition and binding. Therefore, the variable sequence in the cgRNA, including linkers 1 and 2, and the spacer sequence, played an important role in maintaining the proper structure of cgRNA. Although we have demonstrated that linkers AC_5 and AC_{10} served well in most tested sites, optimization of circular RNA

https://doi.org/10.1038/s41467-025-58367-4

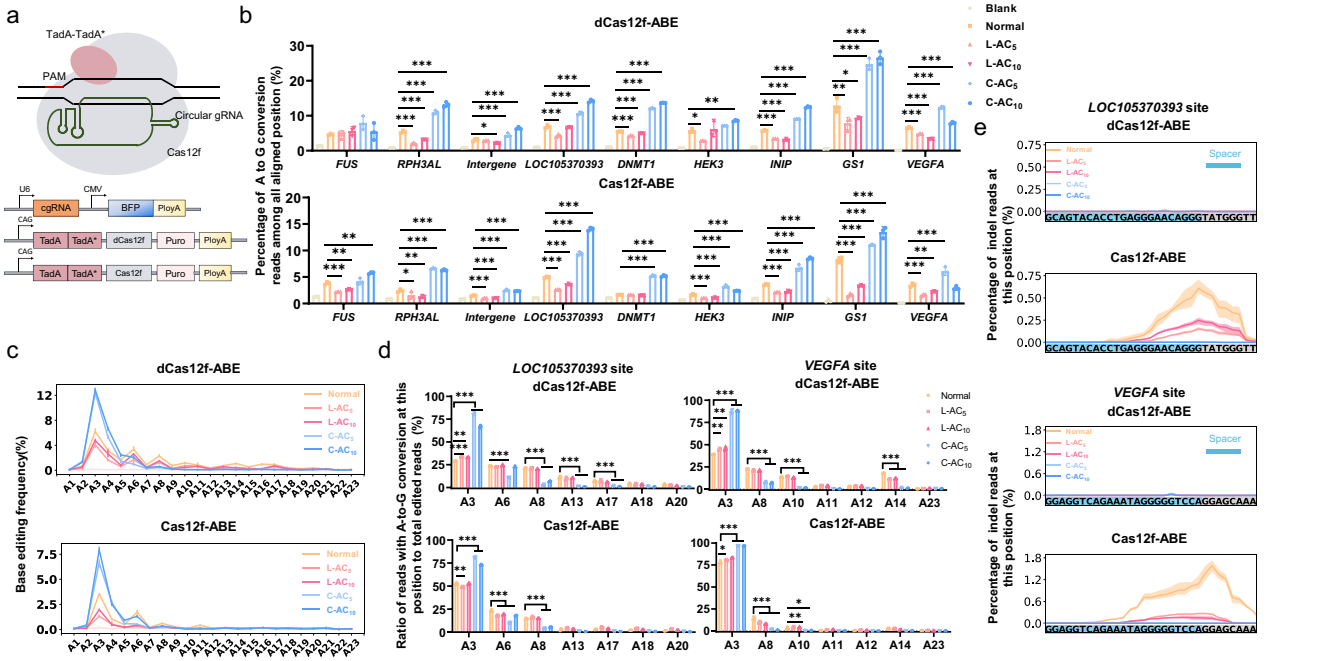

Fig. 5 | Circular gRNAs improve the efficiency and narrow the editing window of A-to-G base editing. a Schematic diagram of A-to-G base editing using the Cas12f/cgRNA system. **b** Deep-seq revealed total A-to-G base editing efficiency at targeted sites in HEK293T cells. The data shown were the percentage of reads with A-to-G conversion out of the total aligned reads. **c** Deep-seq revealed the base editing window in nine target sites. Base editing was applied to edit nine human genomic sites distributed in different chromosomes. The average A-to-G conversion rate of 9 targeted sites was calculated in every A position (A1–A23). **d** Base editing efficiency at each A site in HEK293T cells. The histogram showed the ratio of reads with A-to-G conversion at a specific position to all the edited positions. **e** The indel distribution in *LOC105370393* and *VEGFA* target sites induced by dCas12f-ABE design or Cas12f-ABE design. For **b**–**e** $n = 3$ independent experiments, and data are plotted as mean ± SD $^{*}p < 0.05$, $^{**}p < 0.01$, $^{***}p < 0.001$, one-way ANOVA test, tested sample versus Normal gRNA sample. Source data are provided as a Source Data file.

linkers for a given spacer sequence could be required. We believe that AI-driven structure prediction for RNA, protein, and RNA/protein complex could further improve the editing efficiency of the Cas12f/cgRNA system in the near future.

Methods

Ethics statement

Our research complies with all relevant ethical regulations, and mice experiments were approved by the Scientific Investigation Board of Southern Medical University, Guangzhou, China.

Plasmid construction

For the normal gRNA plasmid, a DNA fragment containing a U6 promoter, a gRNA scaffold, and a gRNA insert site were cloned in the pBluSKM vector with blue fluorescent protein (BFP) driven by a CMV promoter. For the Linear gRNA plasmid, the DNA sequences including a U6 promoter, a 5′ ligation sequence (residues of Twister P3 U2A ribozyme after self-shearing), linker1, a gRNA scaffolds with a gRNA insert site, linker2, and a 3′ ligation sequence (residues of Twister P1 ribozyme after self-shearing) were synthesized and cloned into the pBluSKM vector with the BFP driven by a CMV promoter. For the Circular gRNA plasmid, the DNA sequences including a U6 promoter, a Twister P3 U2A ribozyme sequence, linker1, a gRNA scaffolds with a gRNA insert site, linker2, and a Twister P1 ribozyme were synthesized and cloned into the pBluSKM vector with the BFP driven by a CMV promoter.

For the pCAG-dCas12f-VPR-P2A-mCherry plasmid, the dCas12f (D326A, D510A, D143R, T147R, K330R, and E528R) DNA sequence was synthesized and cloned into the pCAG-d*Lb*Cas12a-VPR-mCherry plasmid backbone. And then inserted the dCas12f-VPR sequence amplified from the pCAG-dCas12f-VPR-P2A-mCherry plasmid into the pBlue-AAVS1-Puro-Cas9:p300-M2rtTA-AAVS1 plasmid, which was dCas12f-VPR knock-in plasmid.

pCAG-TadA-TadA*-dCas12f-P2A-Puro, the synthetic TadA-TadA* DNA fragment, the sequences of dCas12f (D326A, D510A, D143R, T147R, K330R, and E528R) and Puro amplified from the pCAG-dCas12f-VPR-P2A-mCherry and dCas12f-VPR knock-in plasmids, were joined together by DNA assembly. And then mutated dCas12f to Cas12f (D143R, T147R, and E151A) to construct pCAG-TadA-TadA*-Cas12f-P2A-Puro plasmid.

For the pCAG-dCas12f-VPR-sfGFP plasmid, the P2A-mCherry sequence in the pCAG-dCas12f-VPR-P2A-mCherry plasmid was replaced with the sfGFP sequence, amplified from the Pblu-EF1-scFv-GCN4-sfGFP-IDR (FUS)-VP64-GB1-NLS-PA plasmid. Furthermore, the FUS^{IDR} DNA sequence also amplified from the Pblu-EF1-scFv-GCN4-sfGFP-FUS^{IDR}-VP64-GB1-NLS-PA plasmid, was inserted into various loci of the pCAG-dCas12f-VPR-sfGFP plasmid to construct pCAG-dCas12f-VPR-FUS^{IDR}-sfGFP, pCAG-dCas12f-FUS^{IDR}-VPR-sfGFP, and pCAG-FUS-dCas12f-VPR-sfGFP plasmids.

The plasmids pCAG-d*Lb*Cas12a-VPR-mCherry, pBlue-AAVS1-Puro-Cas9:p300-M2rtTA-AAVS1, Pblu-EF1-scFv-GCN4-sfGFP-IDR (FUS)-VP64-GB1-NLS-PA, and luciferase reporter plasmids were described previously.

We designed all gRNA target sites through https://benchling.com/ and ligated them to gRNA expression plasmid. All gRNA sequences are listed in Supplementary Data 1.

Linker design

In order to enhance the circulation and gene editing efficiency of circular gRNA, we designed various 5′ and 3′ linkers with different base lengths and preferences, and then inserted a 5′ linker between the 5′ ligation sequence and the gRNA scaffold, a 3′ linker between the gRNA insert site and the 5′ ligation sequence. And we predicted the circular gRNA structure with different linkers by RNAfold, and selected all which can fold correct ribozyme structure and gRNA scaffold structure. All linker sequences are listed in Supplementary Data 1.

https://doi.org/10.1038/s41467-025-58367-4

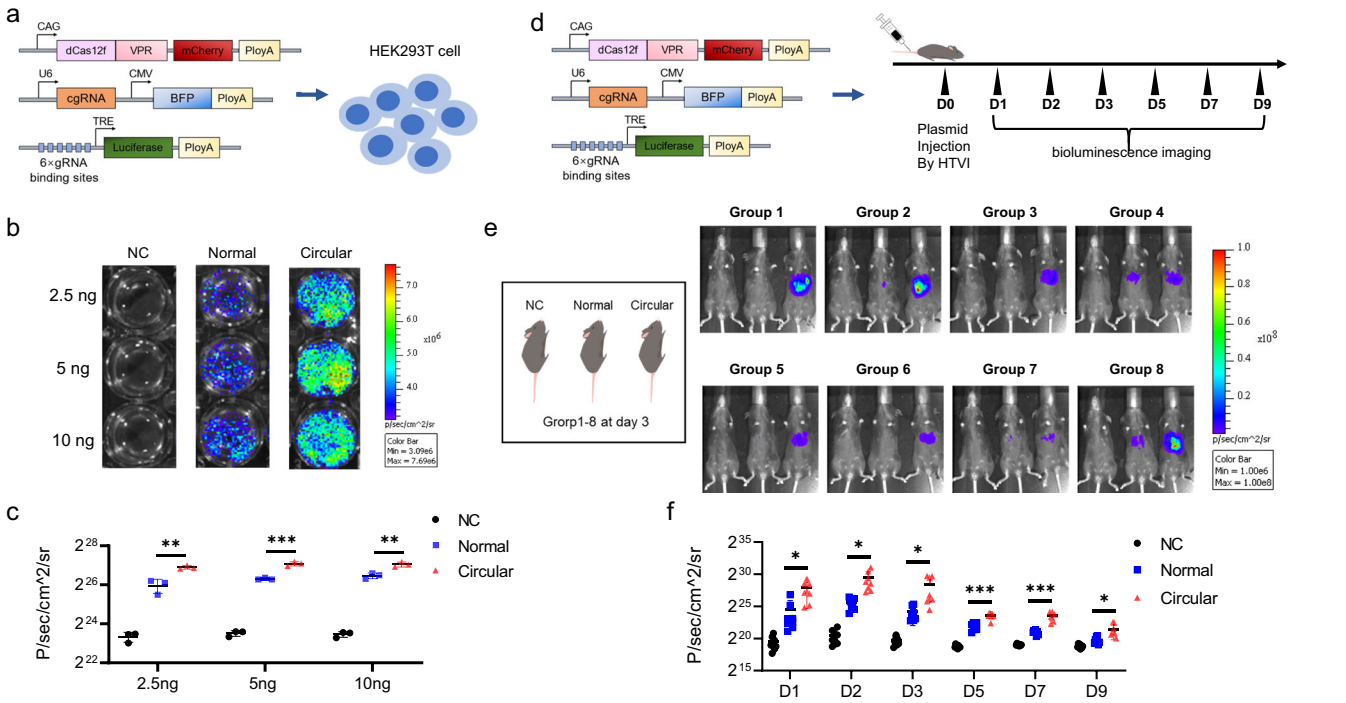

Fig. 6 | Circular gRNAs increase the activation efficiency of dCas12f-VPR in vivo. **a** Schematic representation of luciferase activation using the Cas12f/cgRNA system in HEK293T cells. **b** Bioluminescence imaging showing luciferase activation in HEK293T cells post-treatment with *D*-Luciferin. Data are plotted as mean ± SD ($n = 3$ independent experiments), $^{*}p < 0.05$, $^{**}p < 0.01$, $^{***}p < 0.001$, two-sided Student's *t*-test. **c** Quantification of bioluminescence in HEK293T cells. **d** Experimental design for activating luciferase expression in mouse liver using dCas12f-VPR. **e** Representative bioluminescence imaging results at day 3 for all the eight groups of mice. **f** Quantification of bioluminescence imaging detected over nine consecutive days. Data are plotted as mean ± SD ($n = 8$), $^{*}p < 0.05$, $^{**}p < 0.01$, $^{***}p < 0.001$, two-sided Student's *t*-test. Source data are provided as a Source Data file.

Cell culture and transfection

HEK293T cells (ATCC, CRL-3216 ™) were maintained in Dulbecco's modified Eagle's medium (DMEM), and MCF-7 cells (ATCC, HTB-22), THP1 cells (ATCC, TIB-202), and MV4-11(ATCC, CRL-9591) were cultured in RPMI 1640 medium. All growth media were supplemented with 10% fetal bovine serum (FBS) and 1% penicillin/streptomycin.

For detecting the stability of gRNAs, 24 h after plasmids transfection, we added 5 μg/ ml actinomycin D to cells in 24-well plates, and then harvested cells at certain time points to analyze gRNAs content. For endogenous gene activation, we transfected 16 ng gRNA plasmids and 484 ng pBluSKM vector plasmids to dCas12f-VPR knock-in (KI) HEK293T cell line, and transfected 16 ng gRNA plasmids, 64 ng dCas12f-VPR plasmids and 420 ng pBluSKM vector plasmids to MCF cell line in 24-well plates, then cells were harvested at 3 days post transfection. For THP1 and MV4-11 cell lines, 100 ng gRNA plasmids and 1900ng dCas12f-VPR plasmids were transfected by Lonza kit (Amaxa® Cell Line Nucleofector® Kit SF and SG). For Cas12f/cgRNA system-induced gene activation combined with phase separation, 16 ng gRNA plasmids, 64 ng corresponding dCas12f protein plasmids and 420 ng pBluSKM vector were mixed and co-transfected into HEK293T cells to test targeted gene activation. For DNA base editing assay, in 24-well plates, cells were transfected with 16 ng gRNA plasmids and 484 ng dCas12f-ABE or WT Cas12f-ABE plasmids. The transfected cells were harvested 3 days post transfection for Sanger sequence analysis and Deep-seq analysis.

Quantitative real-time PCR

Total RNA was extracted from transfection cells using VeZol Reagent (Vazyme Biotech) according to the protocol. cDNA was transcribed from 500 ng RNA using HiScript II Q RT SuperMix for qPCR (Vazyme Biotech). cDNA was diluted 20-fold and 2.0ul diluted cDNA was used for each RT-PCR reaction with Taq Pro Universal SYBR qPCR Master Mix (Vazyme Biotech) and run on the Lightcycler 96 (Roche). All primers are listed in Supplementary Data 1.

RNA-seq

The dCas12f-VPR knock-in (KI) HEK293T cells were transfected with 16 ng gRNA and 484 ng pBluSKM vector plasmids and harvested 3 days post transfection. Briefly, RNA was extracted and fragmented to suitable size. Then the first strand of cDNA was synthesized by using random hexamer primers, and followed by the synthesis of the second cDNA strand via PCR, resulting in double-stranded cDNA (ds cDNA). The ends of the ds cDNA were subsequently repaired to be blunt and phosphorylated, preparing them for adapter ligation. After ligating sequencing adapters to these prepared ends, the cDNA underwent a purification process to eliminate unligated adapters and other impurities, thus providing high-quality input for further PCR amplification. The enriched cDNA library, created using specific primers, was sequenced using an Illumina HiSeq instrument with a 150 bp paired-end module. Paired-end reads were compared with HBG gene expression from publicly available databases. Differentially expressed genes of significance were confirmed through the false discovery rate (FDR) < 0.05 and the fold change >2.

Sanger-seq

The transfected cells as described above were harvested using lysis buffer with proteinase K (New England Biolabs) following the manufacturer's protocol. The targeted genome regions of interest were amplified for Sanger-seq, then analyzed by BioEdit.

Deep-seq

The transfected cells were harvested following the manufacturer's protocol. The targeted genome regions of interest were amplified with first rounds PCR by Gold Medal Mix (Tsingke Biotechnology) to add

unique barcodes, and then followed by gel electrophoresis to purify. The second round of PCR was proceeded to add Illumina adapters, and purified by gel electrophoresis. Equal amounts of the products were combined to construct a Deep-seq library. Libraries were sequenced with Illumina HiSeq instrument with 150-bp paired-end reads. All reads were first demultiplexed into different samples based on unique barcodes, then trimmed and aligned with the genome to quantify the editing efficiency, including indels, A-T to G-C conversion at each target site. The primers were listed in Supplementary Data 1.

FACS analysis

The transfected cells were subjected by trypsin digestion and washed by Dulbecco's phosphate-buffered saline (DPBS), then resuspended in 500 µl FACS buffer (1X DPBS,0.2%BSA). BFP and mNeonGreen fluorescence were analyzed by BD LSRFortessa™ flow cytometer. Percentage of mNeonGreen positive was calculated as the proportion of mNeonGreen positive cells of total cells. Activation efficiency in BFP+ was calculated as the proportion of mNeonGreen positive cells within the transfected cells (BFP positive).

FRAP and live-cell imaging

On a glass-bottom microwell dish, HEK293T cells were transfected with 500 ng plasmids encoding CRISPR/cgRNA system. 36 h after transfection, cells maintained in DMEM supplemented with 25 mM Hoechst were imaged on the Nikon A1 confocal microscope with a ×60 oil objective. For fluorescence recovery after photobleaching (FRAP) experiment, the droplets with a diameter about 3 µm was selected, which contained a region of interest (ROI) was bleached by a 488 nm line at 80% laser power, a neighboring unbleached region was used as control and a background region. pre-bleaching and post-bleaching frames were recorded at intervals of 3 s and analyzed with NISElements software. Photobleaching rate (r) was calculated as before photobleaching to after of ROI.

Mice

For the luciferase reporter analysis, C57BL/6 female mice purchased from Guangdong Animal Center were placed in a mouse cage with 12 h light /12 h of darkness, room temperature of 25 ± 2 °C, ambient humidity range from 50 to 60%. Each six-week-old mouse was injected with 2.0 ml 0.9% sterile saline that mixed of 10 µg luciferase reporter plasmids, 10 µg pCAG-dCas12af-VPR-mCherry plasmids, and 2.5 µg gRNA plasmids. Fifteen minutes before imaging, each mouse was injected with 100 µl 20 mg/ml D-luciferin potassium salt (Beyotime), and then imaged with 10 s of exposure time. The bioluminescence imaging performed over nine consecutive days. Only female animals were used in this study, because the sex of the animals is not considered relevant for the studies. All mice experiments were approved by the Scientific Investigation Board of Southern Medical University, Guangzhou, China.

Statistics and reproducibility

No statistical method was used to predetermine the sample size. For cell line experiments, the cells are randomly seeded in 24-well plates before plasmid transfection, and the allocation of plasmid to individual cells also is not programmed. For mice experiments, the grouping of mice was random. The Investigators were not blinded to allocation during experiments and outcome assessment. Detailed statistical tests and quantitative treatment of data are otherwise described in the relevant figure legends or methods sections. No data were excluded from the analyses.

Reporting summary

Further information on research design is available in the Nature Portfolio Reporting Summary linked to this article.

Data availability

All sgRNAs, linkers and primers sequences in this study are available in the Supplementary Data 1. The raw and processed data of RNA-seq generated in this study have been deposited in the National Center for Biotechnology Information database under the accession nos. GSE261105, and the raw and processed data of Deep-seq are available in the National Center for Biotechnology Information database under accession nos. GSE260967. Source data are provided with this paper.

References

1. Jinek, M. et al. A programmable dual-RNA-guided DNA endonuclease in adaptive bacterial immunity. *Science* **337**, 816–821 (2012).
2. Barrangou, R. et al. CRISPR provides acquired resistance against viruses in prokaryotes. *Science* **315**, 1709–1712 (2007).
3. Shmakov, S. et al. Diversity and evolution of class 2 CRISPR-Cas systems. *Nat. Rev. Microbiol.* **15**, 169–182 (2017).
4. Mali, P. et al. RNA-guided human genome engineering via Cas9. *Science* **339**, 823–826 (2013).
5. Konermann, S. et al. Transcriptome engineering with RNA-targeting type VI-D CRISPR effectors. *Cell* **173**, 665–676.e614 (2018).
6. Liao, H. K. et al. In vivo target gene activation via CRISPR/Cas9-mediated trans-epigenetic modulation. *Cell* **171**, 1495–1507.e1415 (2017).
7. Heidersbach, A. J., Dorighi, K. M., Gomez, J. A. & Jacobi, A. M. A versatile, high-efficiency platform for CRISPR-based gene activation. *Nat. Commun.* **14**, 902 (2023).
8. Xue, N. & Liu, X. Improving adenine and dual base editors through introduction of TadA-8e and Rad51DBD. *Nat. Commun.* **14**, 1224 (2023).
9. Han, D. & Xiao, Q. Development of miniature base editors using engineered IscB nickase. *Nat. methods* **20**, 1029–1036 (2023).
10. Clow, P. A., Du, M., Jillette, N., Taghbalout, A. & Zhu, J. J. CRISPR-mediated multiplexed live cell imaging of nonrepetitive genomic loci with one guide RNA per locus. *Nat. Commun.* **13**, 1871 (2022).
11. Wang, H., Nakamura, M. & Abbott, T. R. CRISPR-mediated live imaging of genome editing and transcription. *Science* **365**, 1301–1305 (2019).
12. Pickar-Oliver, A. & Gersbach, C. A. The next generation of CRISPR–Cas technologies and applications. *Nat. Rev. Mol. Cell Biol.* **20**, 490–507 (2019).
13. Adli, M. The CRISPR tool kit for genome editing and beyond. *Nat. Commun.* **9**, 1911 (2018).
14. Anzalone, A. V., Koblan, L. W. & Liu, D. R. Genome editing with CRISPR–Cas nucleases, base editors, transposases and prime editors. *Nat. Biotechnol.* **38**, 824–844 (2020).
15. Chavez, M. & Chen, X. Advances in CRISPR therapeutics. *Nat. Rev. Nephrol.* **19**, 9–22 (2023).
16. Wang, J. Y. & Doudna, J. A. CRISPR technology: a decade of genome editing is only the beginning. *Science* **379**, eadd8643 (2023).
17. Kim, D. Y. & Lee, J. M. Efficient CRISPR editing with a hypercompact Cas12f1 and engineered guide RNAs delivered by adeno-associated virus. *Nat. Biotechnol.* **40**, 94–102 (2022).
18. Xu, X. et al. Engineered miniature CRISPR-Cas system for mammalian genome regulation and editing. *Mol. cell* **81**, 4333–4345.e4334 (2021).
19. Hino, T. et al. An AsCas12f-based compact genome-editing tool derived by deep mutational scanning and structural analysis. *Cell* **186**, 4920–4935.e4923 (2023).
20. Kong, X. et al. Engineered CRISPR-OsCas12f1 and RhCas12f1 with robust activities and expanded target range for genome editing. *Nat. Commun.* **14**, 2046 (2023).
21. Karvelis, T. et al. PAM recognition by miniature CRISPR-Cas12f nucleases triggers programmable double-stranded DNA target cleavage. *Nucleic acids Res.* **48**, 5016–5023 (2020).

22. van Haasteren, J., Li, J., Scheideler, O. J., Murthy, N. & Schaffer, D. V. The delivery challenge: fulfilling the promise of therapeutic genome editing. *Nat. Biotechnol.* **38**, 845–855 (2020).
23. Kim, D. Y. et al. Hypercompact adenine base editors based on a Cas12f variant guided by engineered RNA. *Nat. Chem. Biol.* **18**, 1005–1013 (2022).
24. Han L., Hu Y., Mo Q., Yang H. Engineering miniature IscB nickase for robust base editing with broad targeting range. *Nat. Chem. Biol.* **20**, 1629–1639 (2024).
25. Zhang, X. et al. MiniCAFE, a CRISPR/Cas9-based compact and potent transcriptional activator, elicits gene expression in vivo. *Nucleic Acids Res.* **49**, 4171–4185 (2021).
26. Ran, F. A. et al. In vivo genome editing using staphylococcus aureus Cas9. *Nature* **520**, 186–191 (2015).
27. Wu, T., Liu, C. & Zou, S. An engineered hypercompact CRISPR-Cas12f system with boosted gene-editing activity. *Nat. Chem. Biol.* **19**, 1384–1393 (2023).
28. Xin, C. et al. Comprehensive assessment of miniature CRISPR-Cas12f nucleases for gene disruption. *Nat. Commun.* **13**, 5623 (2022).
29. Ma, H. et al. CRISPR-Cas9 nuclear dynamics and target recognition in living cells. *J. Cell Biol.* **214**, 529–537 (2016).
30. Chen, R. & Wang, S. K. Engineering circular RNA for enhanced protein production. *Nat. Biotechnol.* **41**, 262–272 (2023).
31. Wesselhoeft, R. A., Kowalski, P. S. & Anderson, D. G. Engineering circular RNA for potent and stable translation in eukaryotic cells. *Nat. Commun.* **9**, 2629 (2018).
32. Litke, J. L. & Jaffrey, S. R. Highly efficient expression of circular RNA aptamers in cells using autocatalytic transcripts. *Nat. Biotechnol.* **37**, 667–675 (2019).
33. Costello, A., Lao, N. T., Barron, N. & Clynes, M. Reinventing the wheel: synthetic circular RNAs for mammalian cell engineering. *Trends Biotechnol.* **38**, 217–230 (2020).
34. Katrekar, D. et al. Efficient in vitro and in vivo RNA editing via recruitment of endogenous ADARs using circular guide RNAs. *Nat. Biotechnol.* **40**, 938–945 (2022).
35. Yi, Z. & Qu, L. Engineered circular ADAR-recruiting RNAs increase the efficiency and fidelity of RNA editing in vitro and in vivo. *Nat. Biotechnol.* **40**, 946–955 (2022).
36. Liu, L. et al. Circular guide RNA for improved stability and CRISPR-Cas9 editing efficiency in vitro and in bacteria. *ACS Synth. Biol.* **12**, 350–359 (2023).
37. Zhang, X. & Wang, X. Engineered circular guide RNAs boost CRISPR/Cas12a- and CRISPR/Cas13d-based DNA and RNA editing. *Genome Biol.* **24**, 145 (2023).
38. Liang R., et al. Prime editing using CRISPR-Cas12a and circular RNAs in human cells. *Nat. Biotechnol.* **42**, 1867–1875 (2024).
39. Boija, A. et al. Transcription factors activate genes through the phase-separation capacity of their activation domains. *Cell* **175**, 1842–1855 (2018).
40. Ma, S. & Liao, K. Phase-separated DropCRISPRa platform for efficient gene activation in mammalian cells and mice. *Nucleic Acids Res.* **51**, 5271–5284 (2023).
41. Liu, J. & Chen, Y. CRISPR-assisted transcription activation by phase-separation proteins. *Protein Cell* **14**, 874–887 (2023).
42. Xiao, R., Li, Z., Wang, S., Han, R. & Chang, L. Structural basis for substrate recognition and cleavage by the dimerization-dependent CRISPR-Cas12f nuclease. *Nucleic Acids Res.* **49**, 4120–4128 (2021).
43. Landrum, M. J. et al. ClinVar: public archive of interpretations of clinically relevant variants. *Nucleic Acids Res.* **44**, D862–D868 (2016).
44. Wu, Z., Zhang, Y. & Yu, H. Programmed genome editing by a miniature CRISPR-Cas12f nuclease. *Nat. Chem. Biol.* **17**, 1132–1138 (2021).

Acknowledgements

This work was funded by the National Key R&D Program of China (2020YFA0113300 to M.W., and 2022YFA0806303 to Z.R.), the National Natural Science Foundation of China (82070002 and 82370078 to Z.R., 82072329 and 82370003 to Y.L., 82304008 to Z.X., and 82102443 to T.H.), the Major Project of Guangzhou National Laboratory (GZNL2023A03004 to Z.R.), the GuangDong Basic and Applied Basic Research Foundation (2023B1111050005 and 2024A1515012753 to Z.R., 2023A1515012269 and 2022A1515011091 to Y.L. and 2022A1515111046 to X.Z.). Additionally, we gratefully acknowledge Professor Meng Zhao from Sun Yat-Sen University and Dr. Ruoyang Shao from Nanfang Hospital affiliated with Southern Medical University for providing the THP1, MV4-11, and K562 used in this study.

Author contributions

Z.R., Y.L. (Ying Lin), X.Z., and M.L. conceived the idea, designed the experiments, analyzed the data, and wrote the manuscript. X.Z. and M.L. performed most experiments. J.W. performed computer-assistant linker design and screening. K.C. and Y.L.2 (Yuchen Liu) performed bioinformatics analysis for Deep-seq and RNA-seq. J.L., H.H., Y.Z., T.H., S.M., K.L., and J.Z. constructed some plasmids. M.W. read and improved the manuscript.

Competing interests

The authors declare no competing interests.

Additional information

Supplementary information The online version contains supplementary material available at https://doi.org/10.1038/s41467-025-58367-4.

Correspondence and requests for materials should be addressed to Ying Lin or Zhili Rong.

Peer review information *Nature Communications* thanks Yong-Sam Kim and the other, anonymous, reviewer(s) for their contribution to the peer review of this work. A peer review file is available.